

Optical, electrical, and photovoltaic properties of PbS thin films by anionic and cationic dopants

Mohsen Cheraghizade¹ · Farid Jamali-Sheini² · Ramin Yousefi³

Received: 22 November 2016 / Accepted: 26 March 2017 / Published online: 3 May 2017
© Springer-Verlag Berlin Heidelberg 2017

Abstract Lead sulfide (PbS) thin films were deposited by CVD method to examine the effects of anionic and cationic dopants on optical and electrical properties for photovoltaic applications. XRD diffractograms verified the formation of cubic phase of multicrystalline PbS thin films. FESEM images showed surface morphologies in nano-dimensions (rods and flowers). UV–Vis–NIR spectrum revealed absorbance in the visible and NIR regions for all samples, in which dopants decreased the intensity of absorbance. Se as an anionic dopant for PbS thin films increased electrical resistance, acceptor concentrations, and crystallite defects, and decreased flat-band voltage and depletion width. Finally, photovoltaic measurements indicated that Zn-doped PbS thin film, as a photovoltaic cell, exhibited higher conversion efficiency and external quantum efficiency (EQE).

1 Introduction

At present, humanity faces a global energy problem due to inescapable depletion of fossil fuels and the increasing energy demand required to support the current models of economic growth. Moreover, utilization of fossil fuels leads

to prevalence of infection problems, which is of great significance today. Among a number of alternative resources, renewable energies are rapidly becoming the leading solution to meet the growing needs of power sources. However, with respect to the renewable energy sources, solar energy is considered as the most promising one. Every day the sun shines on the earth, thus providing around 3×10^{24} J of green energy per year [1]. This amount of energy is equal to 4.9×10^{14} barrels of crude oil.

Solar cells can be easily installed anywhere and can produce electrical energy. For example, they can easily provide the electric power of telecommunication towers that are installed in the desert and arduous areas. The present solar cells are mainly made up of semiconductor materials. Hence, conducting any research addressing the properties of semiconductors used in solar cells plays a prominent role to shed more light on the issue. Due to near-optimal energy band gap and high optical absorption coefficient, PbS can be considered as an amazing preferred material that has recently received great attention as a potential material to be used in photovoltaic cells (PVCs) [2–4].

Previous studies revealed that metallic elements of periodic table could improve the electrical properties of semiconductors by increasing the carrier concentration and mobility and decreasing electrical resistance as optoelectronic applications [5–9]. The reason behind the mentioned observation can be related to the fact that metals created donor levels in the electronic band structures of semiconductors, which could lead to the improvement of their electrical conductivity and optical efficiency. Moreover, energy band gap engineering can be performed by doping, so that proper band gap addressing specific goals can be obtained.

Literature review provides a study addressing Se-doped PbS nanostructures, which was conducted by the present research group. The mentioned study revealed that un- and

✉ Mohsen Cheraghizade
mcheraghizade@iauhvaz.ac.ir; mcheraghizade@yahoo.com

¹ Young Researchers and Elite Club, Ahvaz Branch, Islamic Azad University, Ahvaz, Iran

² Advanced Surface Engineering and Nano Materials Research Center, Department of Physics, Ahvaz Branch, Islamic Azad University, Ahvaz, Iran

³ Department of Physics, Masjed-Soleiman Branch, Islamic Azad University (IAU), Masjed-Soleiman, Iran

Se-doped PbS thin films were deposited by physical vapor deposition (PVD) on silicon substrates [10]. The obtained results with respect to morphology of nanostructures showed that Se as a dopant increased the size of structures. However, more reports considering Zn-doped PbS have been provided in the literature. The present research group also examined the effect of Zn atoms on optical properties by PVD method. The optical measurements showed that Zn dopants blue shifted the emission bands and absorbance of optical energy band gap of PbS due to substitution of Pb atoms. Chen et al. [11] synthesized and investigated the effect of Zn impurities on the electrochemical adsorption of butyl xanthate on a galena (alternative name of PbS) surface by chemical precipitation. Phase purity of the samples was examined by XRD analysis and the face-centered cubic (FCC) structure was presented for all samples. Adsorption characterizations indicated that Zn did not improve the adsorption of butyl xanthate on the galena surface. Touati et al. [12] synthesized un- and Zn-doped PbS thin films on glass substrates using the chemical bath deposition (CBD) method and investigated their structural and electrical properties. XRD results revealed that Zn impurities decreased crystallite size and increased micro-strain of thin films. Electrical studies indicated the decrease of carrier concentrations and Hall mobility of Zn-doped thin films. The mentioned decrease was attributed to the increases of grain boundaries by Zn atoms. He et al. [13] developed a micelle-assisted wet chemistry route for incorporation of Zn atoms in PbS quantum dots (QDs) under microwave irradiation. They dissected the formation mechanism of un- and Zn-doped PbS QDs in this method. Their studies indicated that Burstein–Moss effect was responsible for blue shift of absorption edge following Zn doping.

The recent developments of PbS thin films in solar cell applications were carried out by many research groups. For example, Brennan et al. [14] deposited PbS QDs thin films by atomic layer deposition (ALD) method. They used an Al₂O₃ barrier layer in cell structure for increasing photovoltaic efficiency. They reported that the improvement in power conversion of PbS thin films as a photovoltaic device is related to the blocking of recombination at the interface of barrier layer and electron transporter–absorber layers. Sagadevan and Sundaram [14] used spin coating method that is very simple and cost effective for deposition of PbS thin films on SiO₂ substrates. Electrical studies showed that both the dielectric constant and dielectric loss of PbS thin films decrease with the increasing frequency. Moreno-García et al. [15] deposited PbS thin films using lead nitrate, thiourea, and proper surfactants using sequential chemical deposition as a solar cell. They utilized the Bi₂S₃ absorber layer for moderating solar cell structures in order to obtain the higher power conversion efficiency. Their measurements showed that the Bi₂S₃ layer has lower

optical energy band gap and this can help the solar cell device to absorb photons that have higher energy and lower wavelengths. Saikia and Phukan [16] used the CBD deposition method and CdS absorber layer for fabrication of PbS-based solar cell. CdS has higher optical band gap energy and is a good absorber layer for moderating PbS-based solar cells. They obtained the efficiency of 1.668% with a total error of 0.047% for this structure.

To the best of our knowledge, examination of photovoltaic properties of PbS thin films using modified chemical vapor deposition methods has not been reported yet. Hence, the aim of the present study was to investigate and present the effects of Se and Zn dopants on optical, electrical, and photovoltaic properties of PbS thin films.

2 Experimental section

2.1 Synthesis

Deposition details are generally similar to those presented in our previous study [17]. In the present study, high-purity lead (Pb) sheets with 1 × 2 cm² dimensions and a thickness of 2 mm were used as substrates. Pb sheets were polished by soft sandpaper and then ultrasonically cleaned in acetone and ethanol for 10 min in each solvent. High-purity sulfur (S₈) powder as a source material, and selenium (Se) and zinc (Zn) powders (all Merck) as dopant source materials were used. For all three samples, the substrates were positioned on the right side of the furnace in an alumina boat at 330 °C. For the first time, on the other side of furnace only sulfur powder (0.2 g) was positioned in an alumina boat at 185 °C to synthesize un-doped PbS thin films. In the subsequent second and third attempts for synthesis of Se- and Zn-doped PbS thin films, Se powder (0.02 g) at 220 °C and Zn powder (0.02 g) at 500 °C were used together with S₈ powder, respectively. In all attempts, the center of horizontal furnace was kept at 500 °C for 1 h. Furthermore, with the application of a rotary vacuum pump, a 25 Torr pressure was maintained inside the tube furnace during sulfuration of the Pb sheets. Moreover, a mixed carrier gas [Ar (90%), H₂ (10%), 60 sccm] was injected into the horizontal tube furnace in all attempts from the beginning to the end of deposition process.

2.2 Characterizations

To ensure the formation of PbS phase, the XRD analysis was carried out using a Siefert ID 3003 system, which had a Cu anode with $k_{\alpha} = 1.5406 \text{ \AA}$. To investigate the surface morphologies, a field emission scanning electron microscope (FESEM) was used by Hitachi S4160 systems. The elemental contents of the samples were measured using

energy-dispersive X-ray spectroscopy (EDX, Quanta 200 F). The absorption spectra of PbS thin films were recorded at room temperature by a Varian Cary 500 UV–Vis–NIR spectrophotometer in the wavelength range of 400–1200 nm. Photoluminescence (PL) spectra were also recorded at room temperature with a UniRAM system, which had a He–Cd laser with an excitation wavelength of 325 nm and a power of 30 mW.

2.3 Device fabrications and characterizations

Photovoltaic device fabrication was performed similar to that reported in previous studies addressing PbTe nanostructures [18]. C–V and Mott–Schottky plots were recorded by a LCR meter (LCR-8000G Series-GW Instek) with a frequency of 1 kHz in the voltage range of 10–600 mV. The solar cell measurement was carried out under 100 mW/cm² (1.5 Air Mass) illumination by a solar simulator (Solar cell simulator IIS-200+, Nanosat Co., Iran). A 100 W xenon lamp served as a light source, and the intensity of light was calibrated using a standard silicon solar cell. The effective surface of the samples exposed to the light was 0.25 cm². To measure and plot *I*–*V*, *J*–*V*, and external quantum efficiency (EQE) graphs, a Keithley source meter 2400 was used.

3 Results and discussion

Phase and crystalline studies of the deposited films were carried out using XRD (Fig. 1a). For all samples, XRD patterns verified the formation of cubic PbS structures according to the standard card of bulk PbS (JCPDS Card No. 05-0592) [19]. With respect to un- and Zn-doped films, Pb peaks were observed in the XRD patterns. Moreover, the

presented XRD patterns verified the formation of multicrystalline PbS thin films on Pb substrates. Dopants shifted XRD pattern peak to the lower (Se) and higher (Zn) positions (Fig. 1b). This shift was associated with the dopant atom incorporation (substitution and/or interstitial) in the crystal lattice of PbS thin films in doped samples, and the lower and higher shifts observed in the peak position were dependent on the effective ionic radius of dopant atoms.

FESEM images at high magnification were obtained to analyze the evolution of surface morphology of PbS thin films. Figure 2 presents FESEM images and EDS spectra of PbS thin films. As presented in the figure for un-doped film (Fig. 2a), there are rod-like and small spherical morphologies with the average diameters of 23 ± 5 and 58 ± 5 nm, respectively. By adding Se and Zn dopants (Fig. 2c, e), flower-like morphologies with the average diameters of 412 ± 5 and 142 ± 5 nm for Se- and Zn-doped PbS thin films were observed, respectively. Hence, it can be claimed that PbS thin films were grown with nano-dimensional surface morphologies, i.e., nano-rods and nano-flowers. Usually, anion and cation concentrations can be considered as the most significant factors to obtain different morphologies in metal chalcogenide nanostructures [20]. Moreover, EDS spectra confirmed the presence of dopant atoms in the doped thin films. According to the thermodynamics process for PbS thin film formation using CVD method, the excess of sulfur can be favorable to improve and suppress the formation of oxide impurities such as PbO [21]. So it seems that sulfur excess can be caused by faster and better vapor–liquid–solid (VLS) process, is a desirable phenomenon that happening.

With respect to the estimated optical band gap energy of PbS thin films, UV–Vis–NIR spectra of the samples were recorded (Fig. 3). This spectrum showed an absorption edge of about 650–750 nm for all samples.

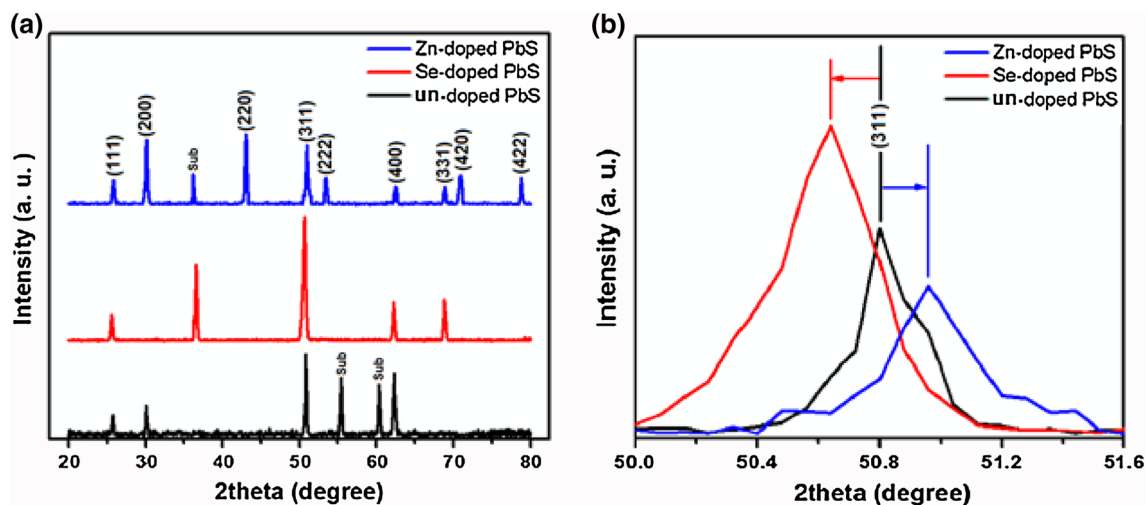


Fig. 1 a XRD patterns and b peak shifting in XRD pattern of PbS thin films

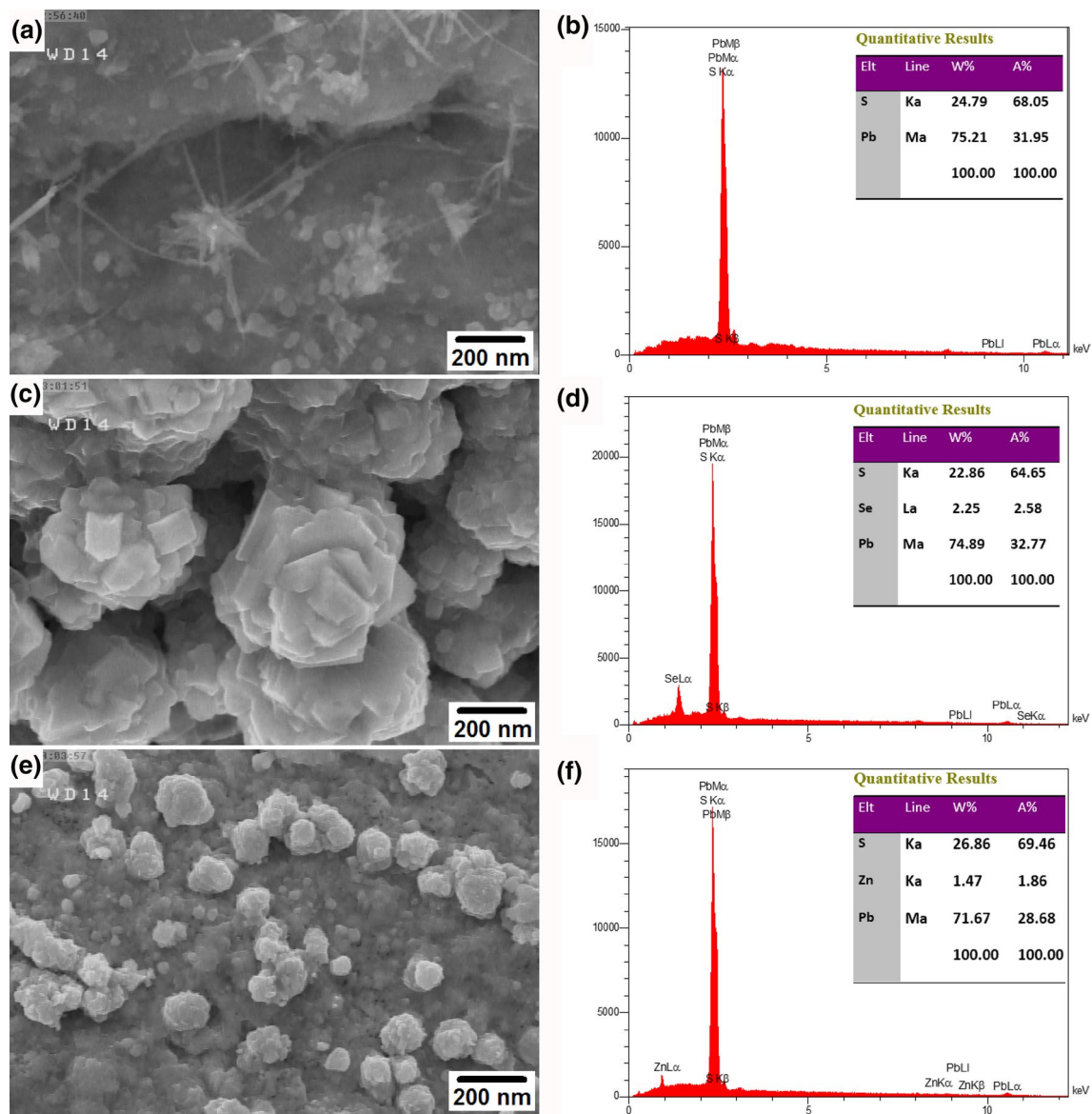


Fig. 2 FESEM images and EDS spectra of **a, b** un-doped, **c, d** Se-, and **e, f** Zn-doped PbS thin films

Intensity of absorbance decreased for PbS thin films by adding dopants. Tauc plot can be considered as a well-recognized and graphical method for estimation of optical energy band gaps of semiconductor materials, which uses Kubelka–Monck model [22]. Figure 4 shows Tauc plots of un-, Se-, and Zn-doped PbS thin films, respectively. Optical energy band gaps of PbS thin films decreased, i.e., red shift in the absorbance edge, by adding Se, and increased, i.e., blue shift in the absorbance edge, by adding Zn dopants.

The red shift for Se-doped and blue shift for Zn-doped PbS nanostructures were observed and reported in our previous study [10] and by He et al. [13], respectively. These shifts are due to the partial formation phase of PbSe (Se-doped PbS) and ZnS (Zn-doped PbS), which have lower

and higher optical energy gaps in comparison with PbS, respectively. The mentioned point can be expressed in terms of the following equations:

$$E_g(\text{PbSe}_x\text{S}_{1-x}) = (1-x) \times E_g(\text{PbS}) + x \times E_g(\text{PbSe}) \quad (1)$$

$$E_g(\text{Pb}_{1-x}\text{Zn}_x\text{S}) = (1-x) \times E_g(\text{PbS}) + x \times E_g(\text{ZnS}). \quad (2)$$

To conduct more investigations about the optical properties of PbS thin films and to study the effects of dopants, PL spectra were examined (Fig. 5). PL spectra of all samples showed three main band emissions. For the un-doped sample, the first band emission observed in the green regions

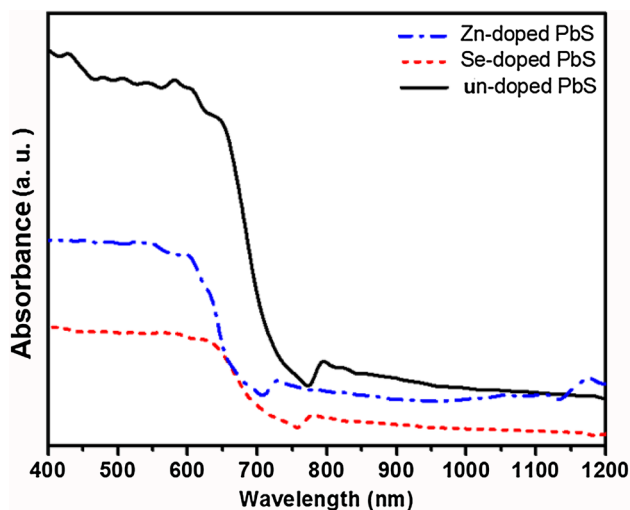


Fig. 3 Absorbance spectra of un-, Se-, and Zn-doped PbS thin films

of visible wavelengths can be attributed to excitonic transitions, which might have been originated from the transition of increased S vacancy donors to recombine with interstitial S acceptors in the valence band [23]. The second band emission located in the red region was attributed to the small size of agglomerated particles, which was an evidence for the growth of PbS thin films with nano-dimensional surface [24]. Finally, the third band emission located in the near-infrared (NIR) region was attributed to the band edge emission of PbS thin films, which was in accordance with the absorption spectra of PbS thin films.

Band edge emissions in the PbS thin films were associated with the transition of electrons from the conduction band edge to the holes trapped at interstitial Pb^{2+} sites [25]. The intensity of PL band emission in doped PbS thin films was higher than that of un-doped films. It is probably due to decreased surface traps, which highly enhanced the intensity of band emission in PL spectra by elimination of non-radiative relaxation of electron transition [23]. As a result, the main conclusion with respect to the samples of the present study is that Zn-doped PbS revealed more defects. With regard to red and NIR band emissions, red (higher wavelengths) and blue (lower wavelengths) shifts were observed for Se- and Zn-doped PbS thin films, respectively. The mentioned shifts are indicative of dopant effects on PbS thin films and are mentioned in the previous section (Eqs. 1, 2).

Electrical properties of PbS thin films were investigated by I - V and Mott-Schottky methods. Based on I - V plots (Fig. 6), electrical resistance of PbS thin films increased by Se and decreased by Zn dopants in dark and illumination conditions. The mentioned plots showed a good rectification for all samples with the lowest turn-on voltage for Zn-doped and the highest turn-on voltage for Se-doped PbS

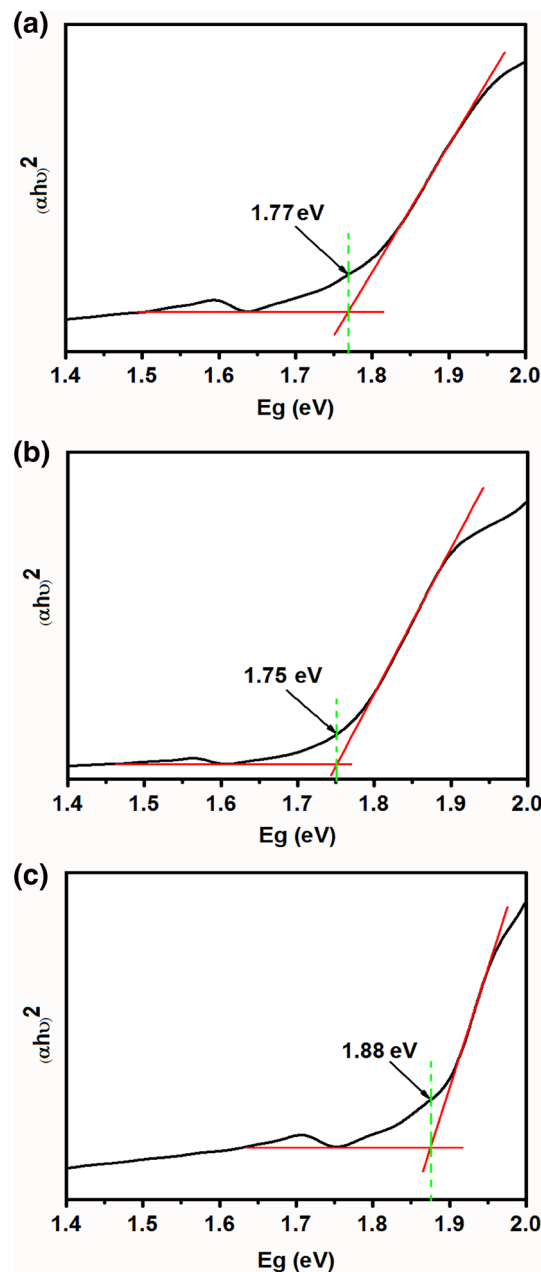


Fig. 4 Tauc plots for the estimation of optical band gap energy of a un-, b Se-, and c Zn-doped thin films

thin films. Capacitance–voltage and Mott–Schottky plots were used to investigate more electrical parameters (Fig. 7). Capacitance properties can be attributed to the existence of depletion region and are characteristics of semiconductors in the case of applying a potential difference to them. Se-doped PbS thin films had a higher capacitance value because of higher electrical resistance and lower electrical conductivity as presented in I - V plots.

Physical parameters obtained from the Mott–Schottky plots (Fig. 7b) were based on the equations presented in

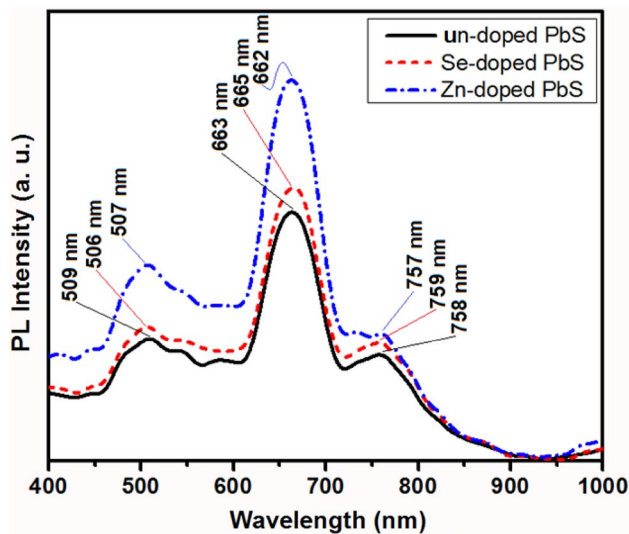


Fig. 5 PL spectra of PbS thin films

our previous study [26] (Table 1). *P*-type conductivity of all films was confirmed by the negative slope of these plots [27, 28]. PbS thin films presented the maximum acceptor concentration among the three samples created by anionic (Se) dopants, which was typically dependent on the metal vacancy in metal chalcogenides. To the best of our knowledge, PbS, similar to other metal chalcogenides such as SnS and PbSe, has intrinsic *p*-type conductivity because of Pb deficiency (metal deficiency) such as Pb vacancy and/or interstitial and excess in S interstitials (chalcogenide interstitials) [29, 30]. Hence, it seems that the Se-doped PbS thin film has higher crystalline defects. Higher densities of states in the Se-doped PbS samples and their electrical resistance, which are reflected in the *I*–*V* plots, also confirm these characteristics for Se-doped PbS thin films. Density of states in the valence band exhibited decreases in Zn-doped PbS thin films. The observed decreases in density of states by Zn (metal) dopant for PbS measurements with the application of Hall methods have been reported by Touati et al. [12].

Generally, metal dopants decrease the electrical resistance and increase the electrical conductivity of PbS. Several reasons have been attributed to the improvement of electrical conductivity such as crystallite features and interstitiality and/or substitutionality of metal (dopants) atoms [7, 31–33]. However, in the present study, it seems that the higher electrical resistance of Se-doped PbS thin films is related to the high density of crystalline defects, which act as trap levels and disturb the carrier transportation in the PbS thin films. The mentioned phenomena can significantly enhance the concentration of carriers in the conduction band of PbS thin films [34].

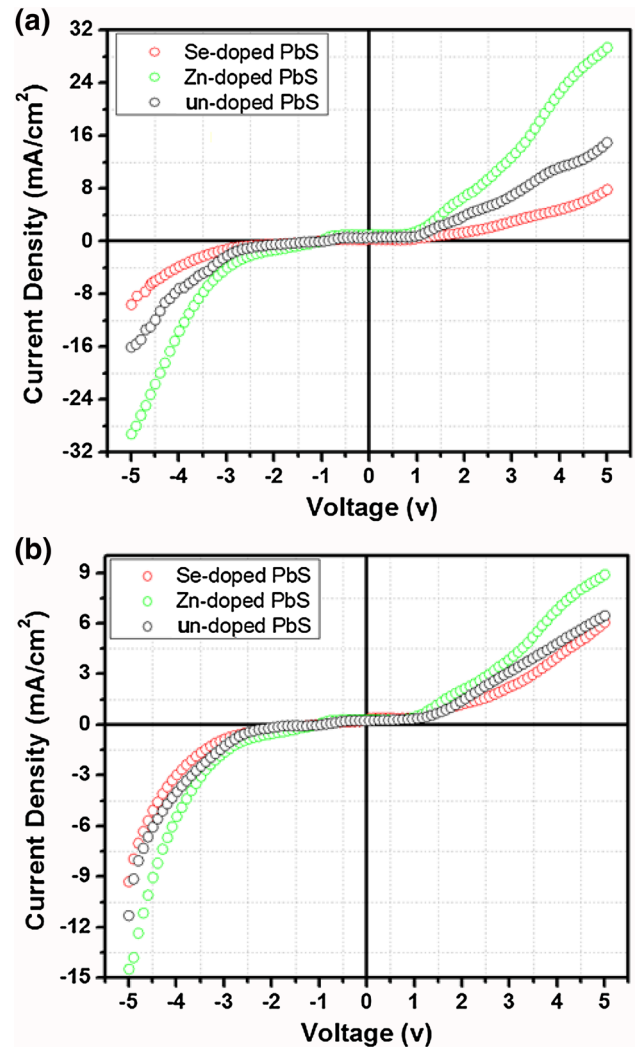


Fig. 6 *I*–*V* characterizations of PbS thin films under **a** dark and **b** illumination conditions

Figure 8 shows the solar cell characteristics (*J*–*V* curve) of un-, Se-, and Zn-doped PbS thin films. Fill factor (FF) and efficiency (η) of a solar cell can be calculated using the following equations [35]:

$$FF = (V_{\max} \times I_{\max}) / (V_{oc} \times I_{sc}) \quad (3)$$

$$\eta = (V_{oc} \times I_{sc} \times FF) / P_{in}, \quad (4)$$

where V_{\max} and I_{\max} are the maximum voltage and current, respectively, using which the maximum power was obtained, V_{oc} is the open circuit voltage, I_{sc} is the short circuit current, and P_{in} is the power of incident light. The FF, efficiency, and other quality parameters were calculated (Table 2). The obtained results showed that the Zn-doped PbS thin film had the highest efficiency and the lowest FF. An FF value less than 0.6 indicates that recombination has occurred in the solar cells, and electron–hole pairs have

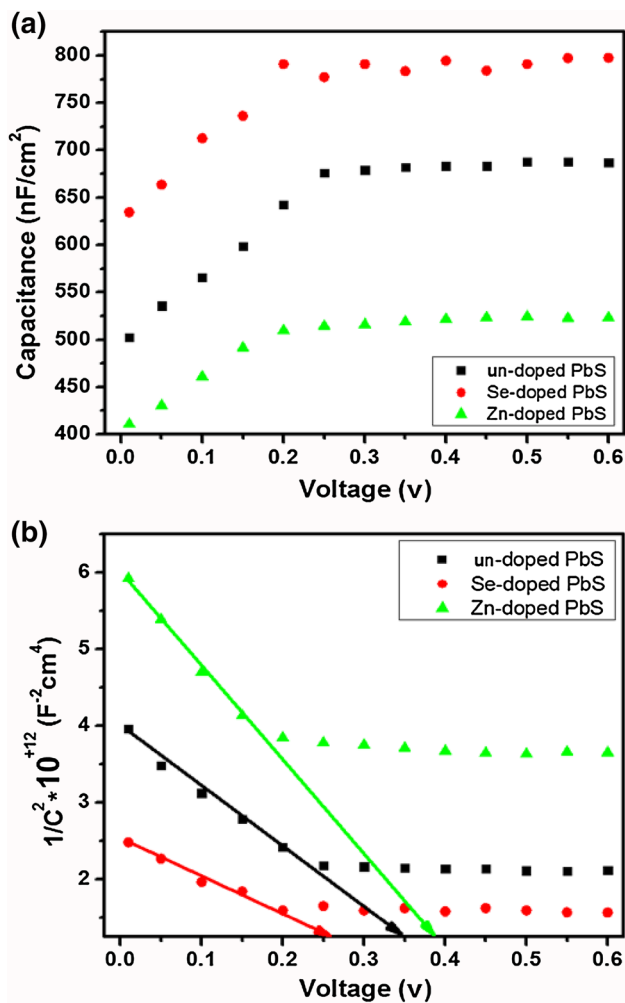


Fig. 7 a C–V and b Mott–Schottky plots of PbS thin films

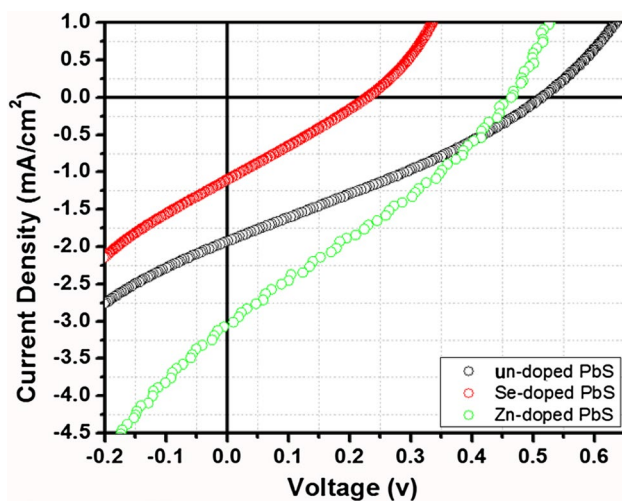


Fig. 8 J–V characteristics of PbS thin film-based solar cells of un-, Se-, and Zn-doped thin films

recombined after the generation and are not transmitted to the external circuit [36]. With respect to binary *p*-type semiconductors such as PbS, FF value was affected by the light absorption and effective hole carrier density of the absorber [37]. The light absorption is strongly dependent on the optical absorbance and band gap of the absorbers. Hence, doping in this research presented as UV–Vis–NIR spectrum also indicated decreases of optical absorbance leading to the reduction of FF.

In contrast to FF, efficiency of PbS thin-film solar cells increased by adding Zn dopants. The important points required to be considered to improve PbS solar cell efficiency are band alignment and density of defect states at PbS/buffer interface, PbS bulk defects and formation of secondary phases, short minority carrier lifetime and diffusion length, PbS back contact, and solar cell configuration [38]. In the present study, the observed lower efficiency and higher series resistance of Se-doped PbS thin films can be ascribed to the high density of defects in this sample, which were verified by the presented *I*–*V* and Mott–Schottky characteristics. Unlike the mentioned high efficiency and lower series resistance of Zn-doped PbS thin film, the obtained result suggests optimum substitution of Zn atoms in Pb sites with minimum interstitials, which improved photovoltaic performances. Depletion width was affected by the interplay between acceptor density and static relative permittivity. Electron–hole pairs were efficiently generated, moved, and separated in the depletion region. Hence, wider depletion width provides higher output current density and higher efficiency in the Zn-doped PbS-based solar cells [39].

To confirm the obtained results addressing photovoltaic characteristics, EQE spectrum of solar devices fabricated for PbS thin films were recorded at various wavelengths (Fig. 9). These spectra showed EQEs of about 58, 51, and 69% for un-, Se-, and Zn-doped PbS-based solar cells, respectively. The solar cells used in this study revealed a good EQE value in the visible and NIR regions of electromagnetic spectrum. The mentioned observation is in good agreement with UV–Vis–NIR spectrum of the samples presented in Fig. 4. Quantum efficiency is defined as the ratio of the number of generation carriers that participated in external current density of device to that of the incident photons. Hence, EQE results also confirmed higher photovoltaic performance of Zn-doped PbS thin films in the present study.

4 Conclusion

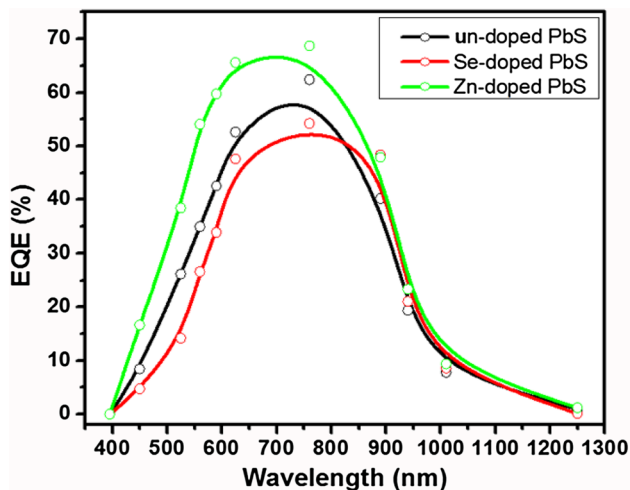
Optical, electrical, and photovoltaic properties of un-, Se-, and Zn-doped PbS thin films, which were synthesized by modified CVD methods, were provided in the

Table 1 Physical parameters obtained from Mott–Schottky plot of PbS thin films

Junction parameters/samples	Un-doped PbS	Se-doped PbS	Zn-doped PbS
Carrier type	<i>p</i>	<i>p</i>	<i>p</i>
V_{fb} : flat-band voltage (v)	0.35	0.26	0.39
N_A : acceptor concentration ($10^{17}/\text{cm}^3$)	6.25	10.10	3.91
V_b : built-in voltage (band bending) (v)	0.35	0.26	0.39
W : depletion width (μm)	0.18	0.08	0.31
N_v : density of states in the valence band ($10^{19}/\text{cm}^3$)	1.43	2.95	0.71
C_v : depletion capacitance ($\mu\text{F}/\text{cm}^2$)	0.16	0.35	9.06

Table 2 Quality parameters of PbS thin films as solar cells

Samples/parameters	V_{oc} (v)	J_{sc} (mA/cm^2)	Fill factor	Efficiency (%)	PCE (%)	R_{ss} (Ω/cm^2)	R_{sh} (Ω/cm^2)
Un-doped PbS	0.52	1.93	0.29	0.29 ± 0.015	5.02 ± 0.251	194.71	308.47
Se-doped PbS	0.23	1.10	0.28	0.07 ± 0.004	1.27 ± 0.064	165.75	183.10
Zn-doped PbS	0.46	3.07	0.25	0.36 ± 0.018	7.06 ± 0.353	141.90	144.81

**Fig. 9** EQE of PbS thin films

present study. Morphological studies revealed that PbS thin films had a nano-dimensional surface morphology of PbS thin films and the dopants changed the surface morphology of films to flower-like in both cases. Optical (emission and absorption) energy band gaps of PbS thin films indicated red and blue shifts by Se and Zn dopants, respectively, which were due to the incorporation of dopant atoms in the crystalline lattice of PbS thin films. Moreover, UV–Vis–NIR and PL results verified the tailoring of energy band gaps. Electrical investigations showed *p*-type conductivities for all samples. In comparison with Se dopant, photovoltaic parameters of PbS thin films were improved by Zn dopant because of lower and higher defects and depletion width, respectively.

Acknowledgements This work was supported by Young Researchers and Elite Club, Ahvaz Branch, Islamic Azad University, Ahvaz (No. 94383). F. Jamali-Sheini and R. Yousefi wish to gratefully acknowledge the financial support of Islamic Azad University, Ahvaz and Masjed-Soleiman Branches to this research work. All the authors express their thanks to Advanced Surface Engineering and Nano Materials Research Center, Ahvaz Branch, Islamic Azad University, Ahvaz, Iran, for their instrumentation support.

References

1. F. Bella, C. Gerbaldi, C. Barolo, M. Grätzel, *Chem. Soc. Rev.* **44**, 3431 (2015)
2. R. Vogel, P. Hoyer, H. Weller, *J. Phys. Chem.* **98**, 3183 (1994)
3. R. Plass, S. Pelet, J. Krueger, M. Grätzel, *U. Bach. J. Phys. Chem. B* **106**, 7578 (2002)
4. N. Zhao, T.P. Osedach, L.-Y. Chang, S.M. Geyer, D. Wanger, M.T. Binda, A.C. Arango, M.G. Bawendi, V. Bulovic, *ACS Nano* **4**, 3743 (2010)
5. P.K. Santra, P.V. Kamat, *J. Am. Chem. Soc.* **134**, 2508 (2012)
6. Z. Huang, X. Zou, H. Zhou, *Mater. Lett.* **95**, 139 (2013)
7. C. Rajashree, A.R. Balu, V. S. Nagarethnam, *Surf. Eng.* **31**, 316 (2015)
8. A. Stavriniadis, A.K. Rath, F.P.G. De Arquer, S.L. Diedenhofen, C. Magén, L. Martinez, D. So, G. Konstantatos, *Nat. Commun.* **4**, 2981 (2013)
9. I. Hod, A. Zaban, *Langmuir* **30**, 7264 (2013)
10. R. Yousefi, M. Cheraghizade, F. Jamali-Sheini, M.R. Mahmoudian, A. Saa'edi, N.M. Huang, *Chin. Phys. B* **23**, 108101 (2014)
11. J. Chen, B. Ke, L. Lan, Y. Li, *Miner. Eng.* **72**, 10 (2015)
12. B. Touati, A. Gassoumi, S. Alfaify, N. Kamoun-Turki, *Mater. Sci. Semicond. Process.* **34**, 82 (2015)
13. X. He, I.N. Demchenko, W.C. Stolte, A. Van Buuren, H. Liang, *J. Phys. Chem. C* **116**, 22001 (2012)
14. S. Sagadevan, A.S. Sundaram, *Chalcogenide Lett.* **11**, 159 (2014).
15. H. Moreno-García, M.T.S. Nair, P.K. Nair, *Thin Solid Films* **519**, 2287 (2011)
16. D. Saikia, P. Phukan, *Thin Solid Films* **562**, 239 (2014)

17. R. Yousefi, M. Cheraghizade, F. Jamali-Sheini, W. J. Basirun, N. M. Huang, *Curr. Appl. Phys.* **14**, 1031 (2014).
18. M.A. Baghchesara, R. Yousefi, M. Cheraghizade, F. Jamali-Sheini, A. Saáedi, M.R. Mahmmodian, *Mater. Res. Bull.* **77**, 131 (2016)
19. International Centre for Diffraction Data (ICDD), (1997)
20. M. Cheraghizade, R. Yousefi, F. Jamali-Sheini, A. Saáedi, N. Ming Huang, *Mater. Sci. Semicond. Process.* **21**, 98 (2014)
21. S.B. Bubenhofer, C.M. Schumacher, F.M. Koehler, N.A. Luechinger, R.N. Grass, W.J. Stark, *J. Phys. Chem. C* **116**, 16264 (2012)
22. F. Jamali-Sheini, R. Yousefi, N. Ali Bakr, M. Cheraghizade, M. Sookhakian, N. M. Huang, *Mater. Sci. Semicond. Process.* **32**, 172 (2015)
23. C. Rajashree, A. R. Balu, *Optik* **127**, 8892 (2016)
24. F. Gao, Q. Lu, X. Liu, Y. Yan, D. Zhao, *Nano Lett.* **1**, 743 (2001)
25. H. Cao, G. Wang, S. Zhang, X. Zhang, *Nanotechnology* **17**, 3280 (2006)
26. F. Jamali-Sheini, M. Cheraghizade, R. Yousefi, *Sol. Energy Mater. Sol. Cells* **154**, 49 (2016)
27. F. Jamali-Sheini, M. Cheraghizade, F. Niknia, R. Yousefi, *MRS Commun.* **6**, 1 (2016)
28. F. Jamali-Sheini, F. Niknia, M. Cheraghizade, R. Yousefi, M. R. Mahmoudian, *ChemElectroChem* (2017)
29. U. Schlichting, K.H. Gobrecht, *J. Phys. Chem. Solids* **34**, 753 (1973)
30. Y. Wang, H. Gong, B. Fan, G. Hu, *J. Phys. Chem. C* **114**, 3256 (2010)
31. K.C. Preetha, T.L. Remadevi, *Physica B* **407**, 4173 (2012)
32. R. Kumar, R. Das, M. Gupta, V. Ganesan, *Superlattices Microstruct.* **75**, 601 (2014)
33. R. Sakthi Sudar Saravanan, M. Meena, D. Pukazhselvan, C.K. Mahadevan, *J. Alloys Compd.* **627**, 69 (2015)
34. B.J. Zheng, J.S. Lian, L. Zhao, Q. Jiang, *Appl. Surf. Sci.* **256**, 2910 (2010)
35. Z. Wang et al., *Polymer* **49**, 4647 (2008)
36. R. Jha, *Solar cell technology and applications*. (Auerbach Publishers, Boca Raton, 2009)
37. D.H. Yeon, S.M. Lee, Y.H. Jo, J. Moon, Y.S. Cho, *J. Mater. Chem. A* **2**, 20112 (2014)
38. J.A. Andrade-Arvizu, M. Courel-Piedrahita, O. Vigil-Galán, *J. Mater. Sci: Mater. Electron.* **26**, 4541 (2015)
39. K.W. Johnston, A.G. Pattantyus-Abraham, J.P. Clifford, S.H. Myrskog, S. Hoogland, H. Shukla, E.J.D. Klem, L. Levina, E.H. Sargent, *Appl. Phys. Lett.* **92**, 122111 (2008)